Journal of Hydrology 519 (2014) 871–880

Contents lists available at ScienceDirect

Journal of Hydrology

journal homepage: www.elsevier.com/locate/jhydrol

Long term variability of the Danube River flow and its relation to precipitation and air temperature

E. Szolgayova [a,*], J. Parajka [b], G. Blöschl [a,b], C. Bucher [a,c]

[a] The Centre for Water Resource Systems, Vienna University of Technology, Karlsplatz 13, 1040 Vienna, Austria
[b] Institute of Hydraulic Engineering and Water Resources Management, Vienna University of Technology, Karlsplatz 13, 1040 Vienna, Austria
[c] Center of Mechanics and Structural Dynamics, Vienna University of Technology, Karlsplatz 13, 1040 Vienna, Austria

ARTICLE INFO

Article history:
Received 28 November 2013
Received in revised form 3 May 2014
Accepted 23 July 2014
Available online 13 August 2014
This manuscript was handled by Andras Bardossy, Editor-in-Chief, with the assistance of Bruno Merz, Associate Editor

Keywords:
Wavelet analysis
Discharge
Precipitation
Cross-wavelets

SUMMARY

In this work the long cycles and long range dependence of monthly discharge, precipitation and air temperature time series from the Danube River during the years 1901–2006 were analysed using wavelet analysis, with emphasis on wavelet coherence and cross wavelet spectra. All time series were deseasonalized prior to the analysis. Long cycles with 11–15 year periods during almost the whole observed period in discharge and during 1935–1975 in precipitation were found. Furthermore a reappearing four year cycle was found in all discharge time series. No significant long cycles were found in the temperature time series, which on the other hand display long term persistence. The cross-wavelet spectra and the wavelet coherence show strong correlation between the precipitation and discharge spectra in the low frequency intervals. Furthermore, a convolution of precipitation and catchment response function was used to examine the propagation of long cycles from precipitation to discharge. The results show, that the long range dependence in precipitation propagates into discharge and that the precipitation lead in the cross-wavelet spectrum increases with the increasing response time. The results indicate that especially mean monthly precipitation could be used as input variable in order to improve stochastic discharge modelling.

1. Introduction

Studies analysing the effect of climate related drivers, such as precipitation and air temperature on discharge are important in order to increase the understanding of the interactions of such process, especially for construction of stochastic models representing long term discharge fluctuations. Within the framework of the ongoing climate change debate, the number of studies analysing the influence of various climate and storage related drivers on discharge has increased in the past years (Blöschl and Montanari, 2010) as a result of the increased interest in the behaviour of discharge over long time scales in general.

Multi-annual cycles and trends have been identified in discharge time series by various methods-filtering techniques and spectral analysis (Pekárová et al., 2003; Probst and Tardy, 1987) or wavelet analysis (Labat, 2008; Sang, 2013). Many studies focused on capturing and describing periodical behaviour of processes from a long term perspective use wavelet analysis. Timuhins et al. (2010), for example found long cycles of 4, 11 and 30 years in Baltic rivers in the past century. Massei et al. (2010) found 5–7 and 17 years cycles in both daily discharge and precipitation for the River Seine in France. Markovic and Koch (2013) examined discharge, precipitation and other variables on several stations for the Elbe River in Germany, finding long cycles in mean monthly discharge and precipitation, but not in temperature. Andreo et al. (2006) found long cycles with periodicities of 2–3 and 4–6 years in monthly precipitation and temperature time series on the Southern Iberian Peninsula. Similarly (Ouachani et al., 2013) found 2–3 and 4–8 years cycles in the seasonal precipitation of Tunisian rainfall.

Several authors examine the influence of climate phenomena, such as the North Atlantic Oscillation on discharge and precipitation. For example (Rimbu et al., 2002) finds, that decadal variations between discharge and precipitation in the lower Danube Basin are "in good agreement" and are "largely controlled" especially by NAO. Mann et al. (1995) find, that decadal atmospheric circulation have high influence on Great Salt Lake levels through precipitation. Markovic and Koch (2013) find significant connection between NAO and mean monthly precipitation on the Elbe River in Germany. At a broader European and Atlantic scale, the influence of NAO on precipitation averages is also well known (Osborn et al.,

* Corresponding author.
E-mail address: szolgayova@waterresources.at (E. Szolgayova).

http://dx.doi.org/10.1016/j.jhydrol.2014.07.047
0022-1694/

1999; Rogers, 1997; Hurell, 1995). More recently, the non-normality and nonlinearity in the multidecadal response of precipitation to NAO have been analysed by Pires and Perdigao (2007) for a large swath of the Northern Hemisphere spanning from the Eastern US to Western Asia. NAO impacts on precipitation have been identified even in regions where the quantities are linearly uncorrelated. However, studies focusing on the influence of precipitation and air temperature on discharge using wavelet analysis are scarce, even though precipitation and temperature are most relevant for hydrological predictions as well (Blöschl and Montanari, 2010). Liu et al. (2011) analysed rainfall and runoff at a half-hourly time step in four experimental catchments in Northwestern China and found the wavelet power spectra of rainfall and runoff to be highly correlated.

Another characteristic used to describe the long term behaviour of time series is long range dependence, i.e. when the autocorrelation function remains significant even for long lags. Long range dependence has been found in daily discharge of European rivers (Szolgayova et al., 2014; Mudelsee, 2007) and daily precipitation time series in Malaysia (Yusof et al., 2013). Skoien et al. (2003) found no long range dependence for precipitation data and some slight long range dependence for discharge in Austria. However, studies examining the relationship between long range dependence and presence of long cycles are lacking.

In order to capture the long term behaviour in discharge modelling knowledge of the long term properties of the time series is of importance. A wide range of stochastic models reflecting the complexity of geophysical processes such as changes in the regime (Bataglia and Protopapas, 2011; Valent et al., 2011; Komorníková et al., 2008), long term persistence (Frolov, 2011; Montanari et al., 2000) or heteroscedasticity (Elek and Markus, 2007; Modarres and Ouarda, 2013) exist. Within the modelling framework, the challenge is to connect the complexity contained in the mathematical models to processes and external drivers (Lee, 2012; Gelati et al., 2010; Fisher et al., 2012). Mann et al. (1995) suggests, that modelling and especially forecasting may be improved, when low frequency events would be more considered in the models. In order to increase the quality of such stochastic models, especially when interested in more process based multivariate models including climate and storage related variables, the interaction of discharge and its drivers needs to be examined as a function of time including long range dependence.

The aim of this paper is to analyse precipitation, air temperature and discharge time series from the upper part of the Danube River in southern Germany, Austria and Slovakia in order to gain understanding of low frequency fluctuations and their interactions and thus explore, whether and how these drivers (especially in monthly time step) could be incorporated into a multivariate discharge model. The following questions will be addressed: What are the statistical characteristics of discharge, precipitation and air temperature as a function of time and do these time series display long range dependence? At what scales and when do the data fluctuate? How are the cycles in discharge related to those in precipitation and temperature?

2. Methods

2.1. Wavelet transform

In this work we are interested in the behaviour of the time series with emphasis on low frequency events. Wavelet transform provides information about the time series for different frequency intervals, making it thus a suitable tool. Furthermore, the wavelet transform does not make the assumption of stationarity of the analysed time series. A continuous wavelet transform of a discrete signal (time series) $X_t,\ t = 0,\dots,T-1$ with a constant time step δt is defined as

$$W_X(s,u) = \sum_{t=0}^{T-1} X_t \psi^*_{s,u}(t) \tag{1}$$

where

$$\psi_{s,u}(t) = \sqrt{\frac{\delta t}{s}}\psi\left(\frac{(t-u)\delta t}{s}\right) \tag{2}$$

is a family of functions obtained through translation and dilation of a mother wavelet $\psi_0(t) \in \mathbf{L}^2(\mathbb{R})$. $(*)$ denotes the complex conjugate, $s \in \mathbb{R}\setminus 0$ is the dilation (scale) parameter and $u \in \mathbb{R}$ is the translation parameter. A wavelet is an arbitrary function localized in time and frequency fulfilling the admissibility condition (Vidakovic, 1999; Torrence and Compo, 1999). The wavelet spectrum is calculated from the wavelet coefficients as $|W_X(s,u)|$. In this work we use the Morlet wavelet $\psi(t) = \pi^{-1/4}e^{i\omega_0 t}e^{-t/2}$, where ω_0 denotes frequency. Even though there are many known wavelet functions (for some examples see e.g. Kaiser (1994)), the Morlet wavelet is very often chosen by practitioners for analysis of geophysical time series (Labat, 2008; Lafreniere and Sharp, 2003; Grinsted et al., 2004; Andreo et al., 2006).

Errors in the wavelet coefficients at the edges of the time series occur due to the finite length of the time series. These errors are taken into consideration by constructing a cone of influence (COI) of the wavelet spectrum. Within the COI such errors are negligible. The cone of influence is given by all points included in the support of the wavelet for each scale. For the Morlet wavelet it is the set of points (u,s) with $u \leqslant \sqrt{2}s$ (Mallat, 1998; Torrence and Compo, 1999).

Statistical significance of the wavelet spectrum is tested assuming the null hypothesis that the time series is randomly generated with autocorrelation properties of red noise. A five percent level of significance is used in the tests.

The global wavelet spectrum is defined as

$$\overline{W}^2_X(s) = \frac{1}{T}\sum_{i=0}^{T-1}|W_X(s,u)|^2 \tag{3}$$

Significant long cycles for each of the time series were tested comparing the global wavelet spectrum to the spectrum of a red noise process for each frequency interval. The red noise spectrum is approximated by an AR(1) process. The AR coefficient is calculated as $(\phi_1 + \phi_2^{0.5})/2$, where $\phi_1,\ \phi_2$ are the lag 1 and 2 correlations of the underlying time series. For details see (Grinsted et al., 2004; Torrence and Compo, 1999).

2.1.1. Cross-wavelet transform and wavelet coherence

Cross-wavelet transform and the wavelet coherence provide information about the relation between two time series. The cross-wavelet transform obtained as

$$W_{X,Y}(s,u) = W_X(s,u)W^*_Y(s,u) \tag{4}$$

can be used as a measure of correlation between the wavelet spectra of two time series $X_t,\ Y_t$. From Eq. (4) the cross-wavelet power is calculated as $|W_{X,Y}|$. Furthermore the phase shift between the analysed series is calculated as the angle of the complex part of the cross-wavelet transform as $arg(W_{X,Y})$.

By normalizing the cross-wavelet transform the wavelet coherence is obtained

$$R_{X,Y} = \frac{|\langle s^{-1}W_{X,Y}(s,u)\rangle|^2}{\langle s^{-1}|W_{X,X}(s,u)|^2\rangle\langle s^{-1}|W_{Y,Y}(s,u)|^2\rangle} \tag{5}$$

where $\langle\cdot\rangle$ is a suitable smoothing operator (Torrence and Webster, 1999). In general $R_{X,Y}(s,u) \in [0,1]$ holds. The significance tests for wavelet coherence and the cross-wavelet spectra are based on Monte Carlo simulations, for details see (Maraun and Kurths, 2004). Here the null hypothesis of no coherence between the two time series is made.

A Matlab package available from (Grinsted et al., 2004) was used for the wavelet and cross-wavelet analysis.

2.2. Hurst coefficient estimation

The Hurst coefficient estimates for discharge, precipitation and temperature were used as complementary information to the wavelet analysis. Time series exhibiting long range dependence exhibit a very slow decrease of the autocorrelation function

$$\rho_\tau \sim C\tau^{2H-2} \quad \tau \to \infty \tag{6}$$

where $\rho_\tau = Corr[X_t, X_{t+\tau}]$ is the autocorrelation function of a weakly stationary time series X_t, C is a constant and $H \in [0,1]$ is the Hurst coefficient. For a stationary process with long range dependence $H \in (0.5, 1]$ holds.

In this work regression on the periodogram and detrended fluctuation analysis were used to estimate the Hurst coefficient. For details on the properties and performance of these two methods see e.g. (Szolgayova et al., 2014; Grau-Carles, 2005). The methods are described in Appendix A.

3. Data

The analysis was performed on four data sets, each consisting of a discharge, precipitation and air temperature time series. The discharge time series from the stations Hofkirchen, Achleiten, Kienstock and Bratislava with catchment areas ranging between from 47,000 to over 131,000 km^2 were used in the analysis (further descriptive statistics including the Hurst coefficient estimates are listed in Table 1).

In order to analyse long term behaviour long series of records are necessary. Thus only series, where sufficiently long precipitation, temperature and discharge data sets are available were used. All time series cover the period between November 1901 and October 2006 (105 years). A monthly time step was used in the analysis. The discharge time series were provided by the Global Runoff Data Center (GRDC, 2011). The precipitation and temperature time series used for analysis were calculated based on data obtained from the European Climate Assessment and Dataset (ECA&D) (Klein Tank et al., 2003). The geographical positions of all stations are shown in Fig. 1.

For each discharge time series catchment area average precipitation time series were constructed using Thiessen polygons (Dingman, 2008). Since the number of available stations changes over time, for the sake of consistency only 16 precipitation stations with sufficiently long records were used for estimating the catchment area averages.

The mean catchment air temperature time series were obtained by linear regression performed for each day of the analysed period, temperature being the dependent and elevation the explanatory variable. The resulting temperature time series were calculated based on the fitted regression coefficients (for each day) using the mean elevation of the respective catchment area. The monthly series were aggregated from thus obtained daily regression series.

No deterministic trend was found in any of the discharge or precipitation time series. Significantly increasing trends were found in all of the temperature series. However, the wavelet analysis and Hurst coefficient estimation results listed and discussed later were conducted on the non-detrended series, since it cannot be distinguished, whether the trend found in the analysed time series is only a part of a cycle with frequency too low to be detected in the data set due to its limited length. It should be noted, that the DFA method already accounts for such trends, thus detrending would not have any effect on the Hurst coefficient estimates using this method. The regression on the periodogram produced significant Hurst coefficient estimates for both detrended and non-detrended time series and the wavelet and crosswavelet spectra were almost trend invariant.

All the time series were deseasonalized prior to further analysis. Let $X_t,\ t = 1, \ldots, T$ be a time series of length T (with monthly time step), the seasonal effects in mean and variance were then removed by subtracting a series of monthly averages and dividing

Table 1
Data description for the four data sets sorted according to the discharge gauge. All four discharge gauges are on the Danube River. For all time series of monthly data the time interval November 1901–October 2006 (105 years) was used. The descriptive statistics are given for non-deseasonalized data. The Hurst coefficients were estimated using the regression on periodogram and the detrended fluctuation analysis (DFA).

	Hofkirchen	Achleiten	Kienstock	Bratislava
General description				
Country	Germany	Germany	Austria	Slovakia
Catchment area, km^2	47,496	76,653	95,970	131,331
Latitude	48.68	48.58	48.38	48.14
Longitude	13.12	13.50	15.46	17.11
Elevation, m	631.06	839.97	827.55	708.63
Descriptive statistics-discharge				
Mean, m^3 s^{-1}	640.72	1426.24	1849.54	2056.38
Standard deviation, m^3 s^{-1}	243.85	537.98	706.60	800.87
Coefficient of variation	0.38	0.38	0.38	0.39
Hurst coeff. – Per.Reg.	0.74	0.71	0.60	0.63
Hurst coeff. – DFA	0.73	0.70	0.67	0.67
Descriptive statistics-precipitation				
Mean, mm	2.52	2.65	2.64	2.38
Standard deviation, mm	1.41	1.41	1.37	1.25
Coefficient of variation	0.56	0.53	0.52	0.53
Hurst coeff. – Per.Reg.	0.66	0.55	0.51	0.43
Hurst coeff. – DFA	0.56	0.51	0.51	0.50
Descriptive statistics-temperature				
Mean, °C	7.86	7.06	6.81	7.45
Standard deviation, °C	7.06	6.90	6.91	7.00
Coefficient of variation	0.90	1.02	1.02	0.94
Hurst coeff. – Per.Reg.	0.72	0.71	0.71	0.72
Hurst coeff. – DFA	0.65	0.65	0.65	0.65

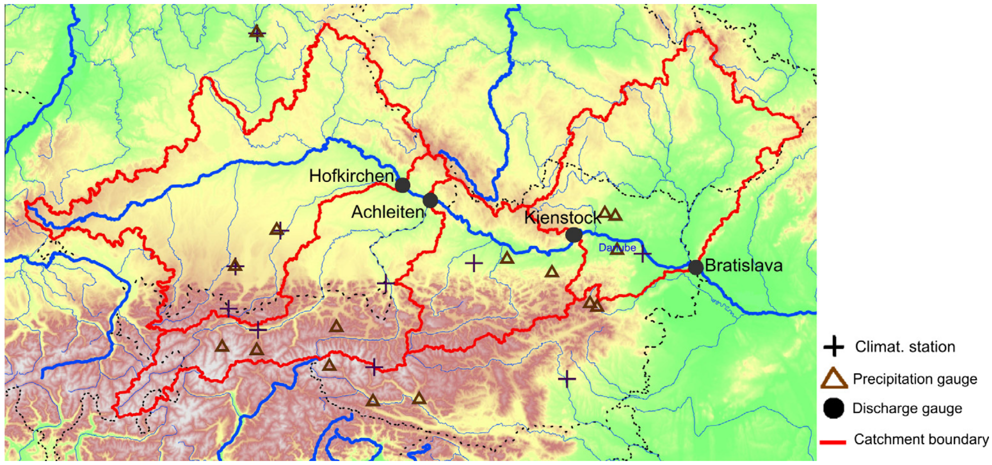

Fig. 1. Geographical position of discharge, precipitation and climatological gauges including the catchment area boundaries.

by the daily or monthly estimated standard deviations respectively as follows (Montanari et al., 2000):

$$X_t^{des} = \frac{X_t - \overline{X}_t}{\sqrt{s_t^2}} \tag{7}$$

with the periodically extended series of monthly averages and estimated variances

$$\bar{X_t} = \frac{1}{n_y}\sum_{i=0}^{n_y-1} X_{(t\bmod 12)+12i} \quad \text{and}$$
$$s_t^2 = \frac{1}{n_y-1}\sum_{i=0}^{n_y-1}\left(X_{(t\bmod 12)+12i} - \bar{X_t}\right)^2 \tag{8}$$

Here $n_y = \lceil T/12 \rceil$ is the number of years.

The catchment average precipitation and air temperature series will be referred to as temperature and precipitation time series in the following for the sake of brevity.

3.1. Discharge convolution

In order to help interpret the relationship between precipitation and discharge and the propagation of low frequency events, a simple convolution calculating discharge from precipitation was constructed. Changing the properties of the convolution function allows to modify the properties of the discharge time series based on a chosen precipitation time series as desired and examine the changes in the cross-wavelet spectrum and the changes in the wavelet coherence. Thus the dependence of discharge on precipitation for different frequencies and time windows can be examined. For this purpose, a daily time step was used. The daily precipitation time series display long range dependence, whereas the monthly precipitation time series behave similarly to a random noise series (see Table 1 and Section 4.1). Thus the use of daily precipitation allows a comparison of the spectra and Hurst coefficients in terms of the long term persistence in precipitation. This would not be possible if monthly series was used.

Discharge series were calculated from precipitation time series for the Hofkirchen and Bratislava by

$$\begin{aligned} Q_t^{gen} &= P_t * \left(\alpha_1 e^{-\alpha_1 t} w_1 + \alpha_2 e^{-\alpha_2 t} w_2\right) \\ &= \int_{-\infty}^{\infty} P_\tau \left(\alpha_1 e^{-\alpha_1 (t-\tau)} w_1 + \alpha_2 e^{-\alpha_2 (t-\tau)} w_2\right) d\tau \end{aligned} \tag{9}$$

where $Q_t^{gen},\ i = 1,2$ is the calculated discharge series, $*$ is a convolution, P_t is the precipitation series, α_i indicate different travel times of water in the catchment and $w_1,\ w_2$ are weights of the respective travel times with $w_1 + w_2 = 1$. Two different travel times with different weights were used in order to simulate a short term (high frequency, short travel time) and a long term (low frequency, long travel time) component of the discharge. In all cases a convolution kernel representing 10 days travel time was combined with long travel time kernels – 1, 5 and 10 years. The long travel times were chosen to be similar to the long cycles found in discharge. Both time series were deseasonalized after the discharge generation analogically to the monthly data sets. The use of deseasonalized data

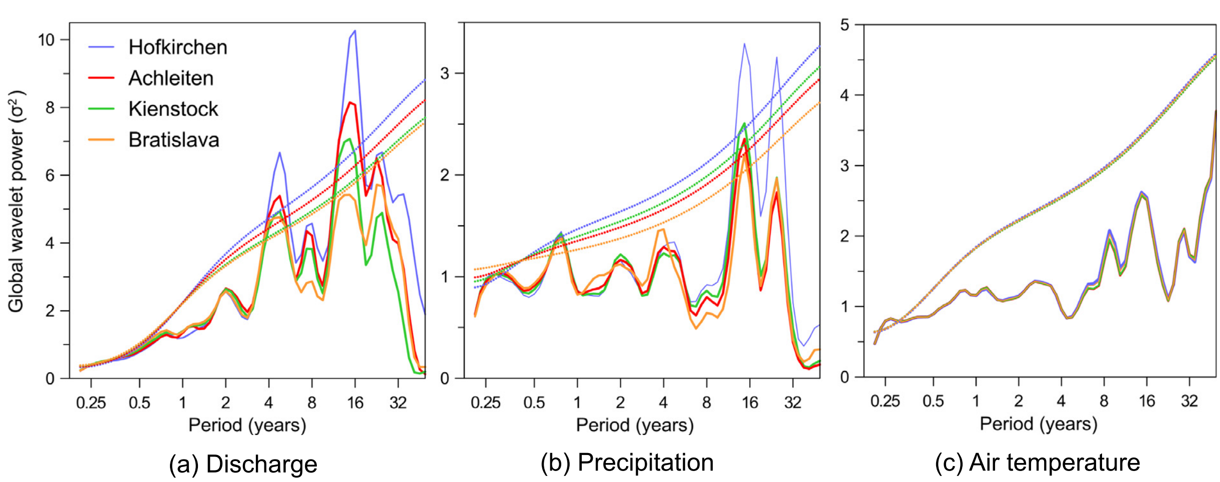

Fig. 2. The global wavelet spectra of the discharge, precipitation and temperature time series. The dotted line represents the 95% confidence bound.

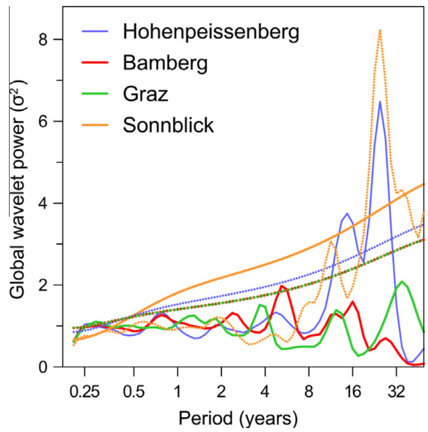

Fig. 3. Example of the global wavelet spectra of mean monthly precipitation time series used for the calculation of the catchment average precipitation series. The dotted lines indicate the 95% confidence bounds of a red noise global wavelet spectrum. (For interpretation of the references to colour in this figure legend, the reader is referred to the web version of this article.)

justifies that snow and soil moisture are not represented in the convolution function.

4. Results

4.1. Long cycles

The graphical output from the global spectrum test can be seen in Fig. 2, the respective spectra for the analysed variables can be found in Fig. 4. On the 95% significance level several long cycles were detected for both discharge and precipitation time series. The global wavelet spectra of the discharge time series (Fig. 2 left) are above the red noise background spectrum for periods between 11 and 15 years for all stations except Bratislava. Cycles with approximately this periodicity are visible in the wavelet spectra for all stations for almost the whole duration of the analysed period. In Achleiten the cycle is significant all the time. Furthermore, for all stations a shorter cycle of 4 years was detected. Based on the wavelet spectra, this shorter cycle is significant only over shorter time periods, for example between the years 1910–1940 and later between 1960 and 1970. All time series display long range dependence with Hurst coefficients larger than 0.7 for the two German stations, and larger than 0.6 for Kienstock and Bratislava for both estimation methods. The Hurst coefficient estimates can be found in Table 1.

All catchment precipitation time series contain a cycle with periods between 11 and 15 years, and on the upstream Hofkirchen station, a long 22 year cycle was detected (Fig. 2 middle). These cycles can be seen on the wavelet spectra as well, even though they vary over time. For all four stations, the 11–15 year cycle is significant approximately between the years 1935–1975. Furthermore, at Hofkirchen, the 22 years cycles is detected as significant until the year 1955. However, the analysis of the autocorrelation functions of all these time series (not shown here) shows, that the autocorrelation structure, especially of the two downstream stations, is very close to white noise and the Hurst coefficients are close to 0.5 in almost all cases accordingly. The decrease of the Hurst coefficient as we move downstream on the Danube River (e.g. H for Hofkirchen is 0.66 and for Bratislava 0.43 using the regression on periodogram method) corresponds to the decrease in the areas significant in power on the precipitation wavelet spectra. In general,

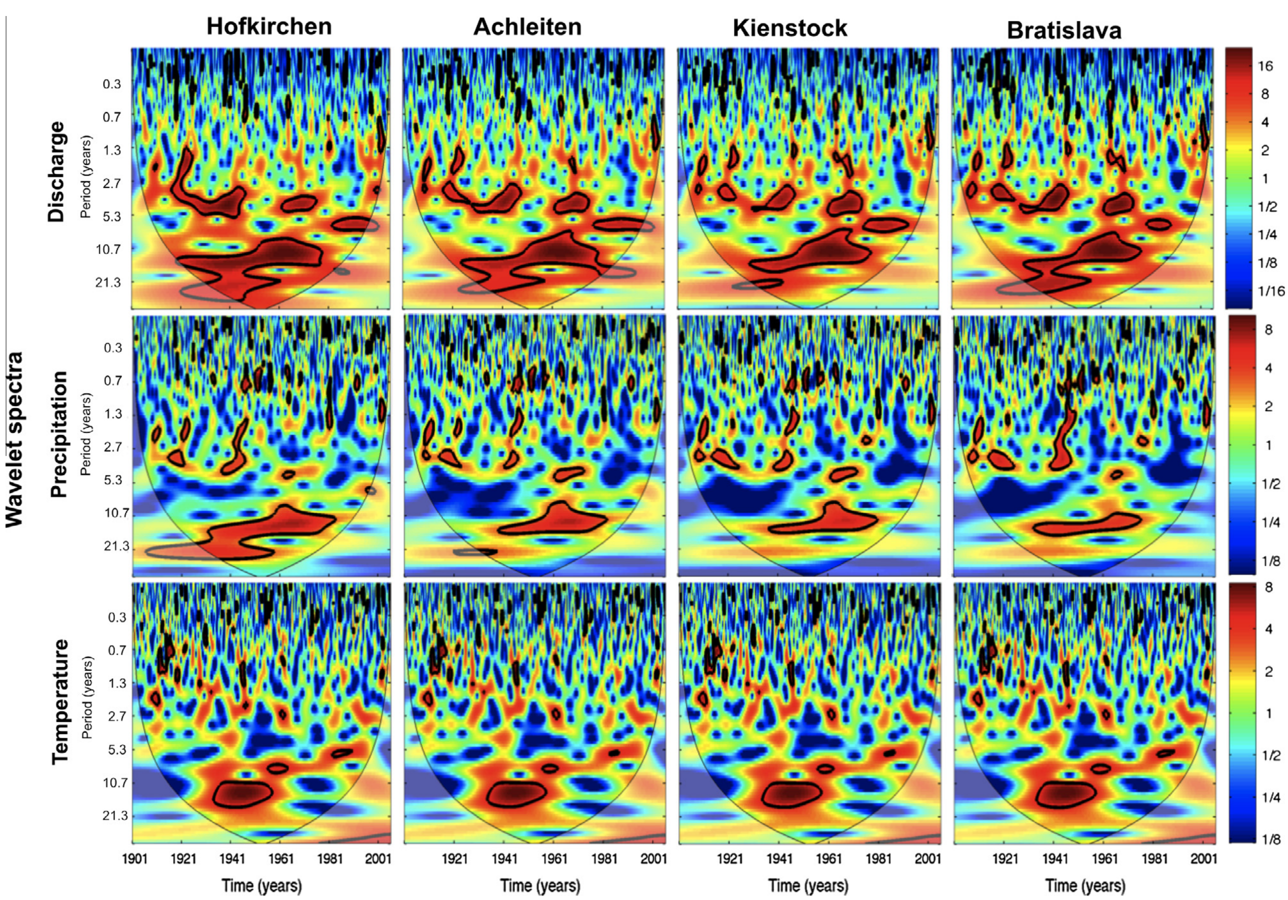

Fig. 4. The wavelet spectra for each of the analysed variables-discharge, catchment average precipitation and air temperature.

the global wavelet spectra of the monthly station precipitation time series used for calculation of the catchment precipitation series show a varied behaviour (see Fig. 3) depending on the geographic position of the climatic stations. Stations in the north east and south west of the considered region contain no significant long cycles. This has an impact on the catchment area averages interpolated from the station time series and on the resulting cycles detected.

The temperature time series do not contain any long cycles compared with the red noise background (Fig. 2 right). Even though the global wavelet spectrum did not indicate any significant cycles, a significant frequency of approximately 10–15 years can be seen from the wavelet spectra of all time series between the years 1935–1955. Furthermore, there is long range dependence present in all four time series: the Hurst coefficients are approximately 0.6 according to the detrended fluctuation analysis and 0.7 according to the regression on the periodogram method. The Hurst coefficients for all time series are almost identical, as are the wavelet spectra (see Fig. 4).

4.2. The cross-wavelet spectra and wavelet coherence

The cross-wavelet spectra and the wavelet coherence spectra can be found in Figs. 4 and 5. The first two rows of Fig. 5 display the cross-wavelet spectra of precipitation and discharge in the first row and temperature and discharge in the second row. The bottom two rows show the respective wavelet coherence spectra.

When comparing the cross-wavelet spectra with the wavelet spectra of the discharge time series, it can be seen that the significant areas of the cross-wavelet spectrum approximately copy the areas significant in the discharge spectra, rather than those of the precipitation spectra for all stations (compare rows one and two in Fig. 4 with the first row of Fig. 5). The time series have both high power for the periods of approximately four years for most of the observed time window. In this period range, precipitation leads discharge by approximately 45° (corresponding to six months lead time) in the first half of the time series until the 1960s. Then, however, we can observe a change in the behaviour for all four analysed data sets and the two time series are in phase until the end

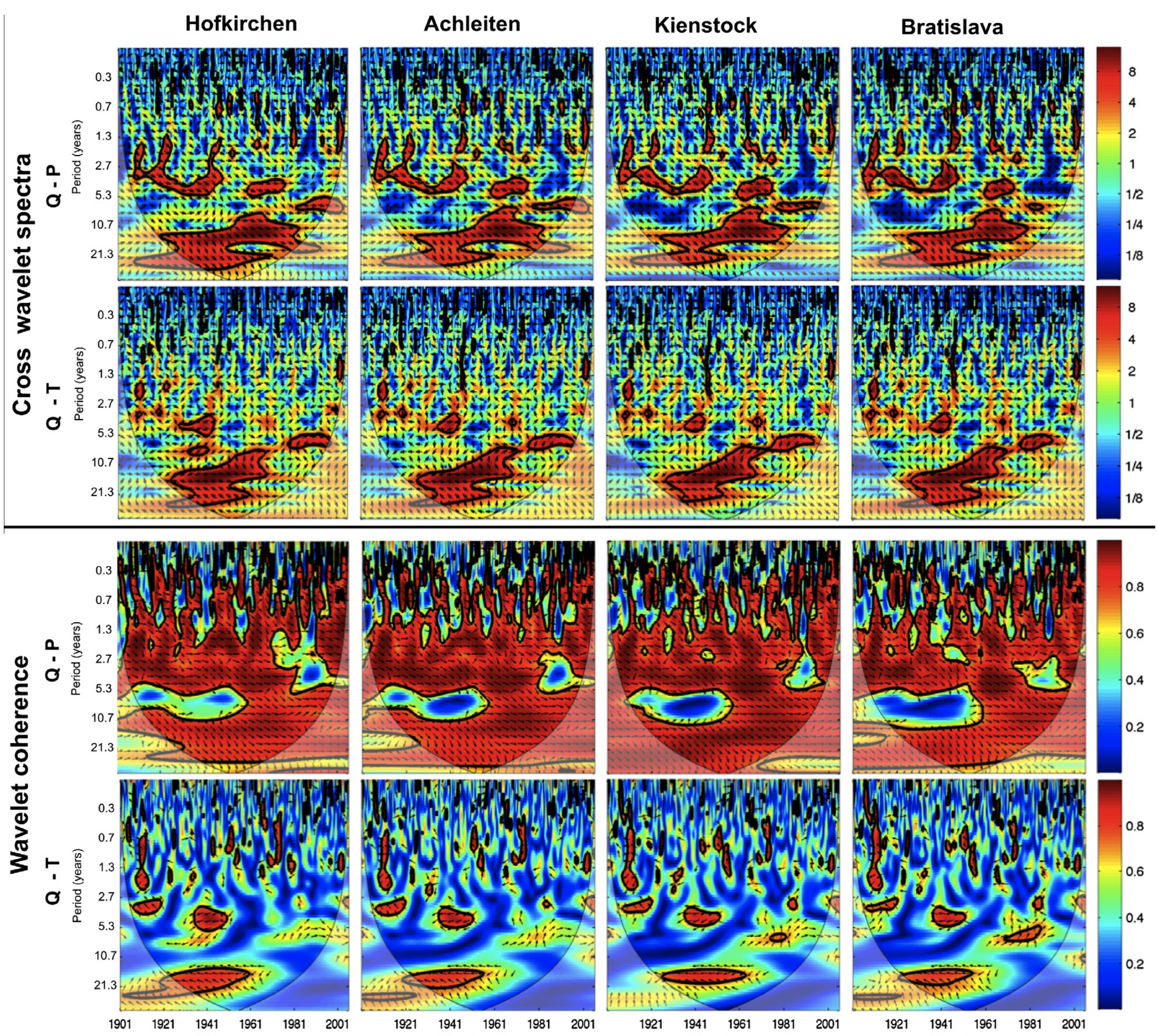

Fig. 5. The cross-wavelet and wavelet coherence spectra. The first two rows show the cross-wavelet spectra between precipitation/discharge and air temperature/discharge respectively. The bottom two rows show the wavelet coherence spectra for the same pairs of variables. Arrows show the phase shift between the respective time series. Colours indicate the measure of coherence – red colour implies high degree of coherence. Arrows pointing right indicate that the two time series are in phase. Arrows pointing down indicate that precipitation/temperature leads discharge. (For interpretation of the references to colour in this figure legend, the reader is referred to the web version of this article.)

of the observation period. In the low frequency area, where the cycles of 11–14 years were observed, the two series are both high in power as well. It can be seen that the lead time of precipitation increases with increasing periodicity of discharge. Here the phase difference changes to almost 90 degrees, which would indicate approximately 3 years lead time. The discharge and precipitation time series show significant degree of coherence for all frequencies for most of the time for all four stations. The time series are almost in phase until the end of the observation period with a lead time of 1–2 months. In the low frequency there is a common area of no coherence for all data sets in the time window 1920–1970 for the period interval between 4 and 11 years.

The temperature spectra display a significant area of power between 1930 and 1960 with the periodicity around 11 years. This time period corresponds to years, where daily air temperature minima were generally below the long time average (compare with an example of the Hofkirchen temperature time series in Fig. 6). This means that the long cycles were present for years with especially cold winters.

A major difference between the temperature–discharge and precipitation–discharge relationships can be seen in the wavelet coherence spectra. The precipitation time series show high levels of coherence for most frequencies and times. On the other hand, the coherence between temperature and discharge is less pronounced at most frequencies and is significant only in the low frequency range. In the temporal periods where the wavelet coherence and the cross-wavelet spectra are significant compared to the red noise background, the temperature and discharge are in anti-phase (20 years periodicity), with increasing period temperature leads discharge by approx. 225° (approximately 13 years leading time). In other areas the phase shifts are random. The significantly coherent period ends in the late 1950s.

4.3. Convoluted data

The goal of the convolution analysis was to gain understanding of the relationship between the long range dependence and the cyclical behaviour in the discharge found in the wavelet spectra. In order to achieve this, several daily discharge time series were calculated using the convolution function described in Section 3.1. Table 2 shows an overview of Hurst coefficients for some of the convoluted time series with various kernel combinations and weights of the kernels used. We see that the Hurst coefficients of the calculated discharge time series increase with the increase of the weight of the long time kernel component. Using only a very long travel time kernel yields a non-stationary process, thus the time series does not fulfill the assumptions of regression on the periodogram estimator, producing $H > 1$ for both estimation methods. The results indicate that the long range dependence in discharge is influenced by the presence of the long range dependence in precipitation (note, that on a 99% significance level the Bratislava precipitation time series does not display long range dependence). However, this influence is not very sensitive to the generator input parameters, since long range dependence was detected in all generated time series, independent of the weight combinations of the kernels. Assuming a convolution function with a dominant long time produces a non-stationary discharge output. Furthermore it seems that with decreasing the travel time of the long term kernel actually produces an increase in the Hurst coefficient. Thus, based on the convolution model, it is not possible to directly attribute the increase in Hurst coefficient to the presence of long cycles (represented by the long time kernel).

An example of the wavelet, cross-wavelet and wavelet coherence spectra of the generated data can be seen in Fig. 7. The time series depicted on the figure was calculated using 5 years travel time with weight 0.9 combined with the 10 days travel time mentioned above, using the Bratislava precipitation time series. Here the estimated Hurst coefficient (using the DFA method) coincides with that of the measured Bratislava daily discharge series. The wavelet coherence is close to 1 for almost all the area of the spectrum. The areas of no significant coherence observed in the real precipitation/discharge time series spectra could be only partially reproduced using this simple generator. The high wavelet coherence is mainly caused by the fact that the discharge time series were directly calculated from the precipitation time series, especially without any added noise. Similarly to the spectra of the observed precipitation/discharge time series, the phase arrows show that for shorter periodicities precipitation leads discharge. In these cases the phase is influenced by the travel time of the water in the catchment. However, the time variability of discharge for longer periods depends on the variability in the precipitation time series, rather than on the travel time. For periodicities bigger than the long time kernel, the phase arrows are not influenced by the weights of each of the kernels. However, for shorter periodicities the increase in lead time of precipitation increases with the increase of the weight of the long time kernel (not shown here).

Table 2
Hurst coefficient estimates for daily convoluted discharge time series. The Hurst coefficients of the real precipitation and discharge time series are listed in the first two rows. Hurst coefficients for different weight combinations and different travel times are listed in the following rows. The Hurst coefficient was estimated using regression on periodogram (Per.Reg.) and detrended fluctuation analysis (DFA).

	Hofkirchen		Bratislava	
	DFA	Per.Reg.	DFA	Per.Reg.
Observed time series				
Discharge	0.91	0.89	0.88	0.89
Precipitation	0.56	0.57	0.54	0.55
Calculated discharge-travel times 10 days, 10 years				
$w_{1years} = 0$	0.76	0.76	0.73	0.73
$w_{1years} = 0.1$	0.76	0.76	0.74	0.73
$w_{1years} = 0.5$	0.77	0.78	0.75	0.74
$w_{1years} = 0.9$	0.85	0.85	0.83	0.80
$w_{1years} = 1$	1.27	1.47	1.24	1.42
Calculated discharge-travel times 10 days, 5 years				
$w_{5years} = 0.1$	0.76	0.77	0.74	0.73
$w_{5years} = 0.5$	0.77	0.78	0.76	0.75
$w_{5years} = 0.9$	0.83	0.86	0.88	0.87
$w_{5years} = 1$	1.06	1.37	1.24	1.42
Calculated discharge-travel times 10 days, 1 year				
$w_{10years} = 0.1$	0.77	0.77	0.74	0.74
$w_{10years} = 0.5$	0.80	0.82	0.81	0.79
$w_{10years} = 0.9$	0.93	1.04	1.03	1.06
$w_{10years} = 1$	1.06	1.36	1.22	1.41

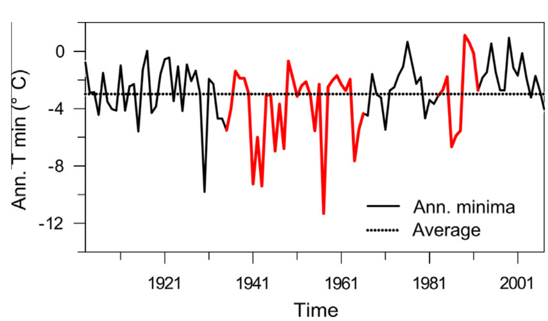

Fig. 6. Daily minimum temperatures for each year for the Kienstock catchment average temperature time series. The red line indicates the time period, where the wavelet spectrum is significant in power for the low frequencies (over 5 years periodicity). (For interpretation of the references to colour in this figure legend, the reader is referred to the web version of this article.)

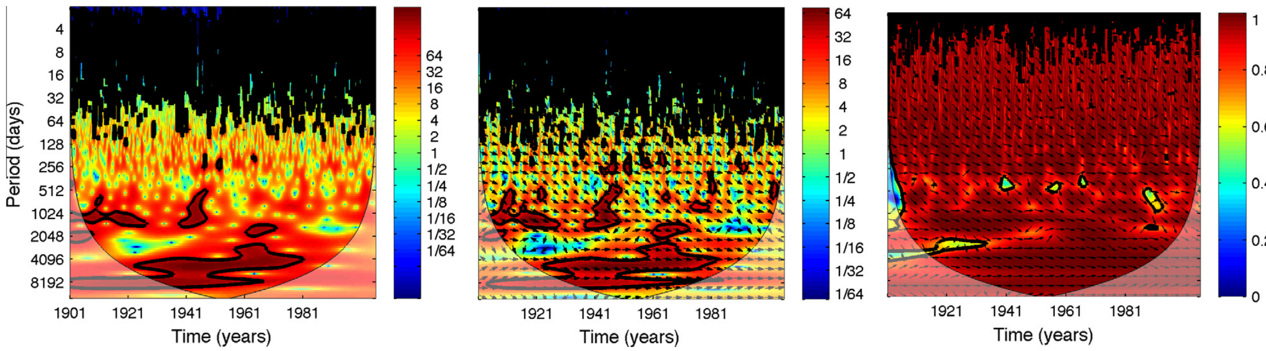

Fig. 7. The wavelet (left), cross-wavelet (middle) and coherence spectra (right) for the discharge time series calculated from the Bratislava precipitation time series using the kernel combining 10 days and 5 years travel times with respective weights 0.1 and 0.9.

5. Discussion and conclusions

The main goal of this paper was to analyse the long term behaviour of mean monthly discharge, temperature and precipitation time series of four stations on the Danube River, with emphasis on long cycles and the dependencies between precipitation, air temperature and discharge. Statistical tests of the global wavelet spectra confirmed a four year cycle in all observed discharge time series on a 95% significance level. Furthermore, long cycles of 11–15 years were detected on the three upstream stations. This is in agreement with (Labat, 2008), who found similar cycles (4, 14, 20 and 33 years) in the annual discharge of the Danube River at Ceatal Izmail in Rumania. It is as well in agreement with findings of other authors, who analysed European discharges and found long cycles – 4 and 11 years cycles on the Baltic rivers (Timuhins et al., 2010) and 10–14 years cycles on the Elbe River (Markovic and Koch, 2013). Rimbu et al. (2002) points out that long cycles, such as those found in the analysed discharge time series are in correlation with positive phase of the NAO and can be associated with below the average sea surface temperature anomalies as well.

Unlike other authors, who found cycles of around 5 years in precipitation data sets on the Iberian Peninsula and North Africa (Andreo et al., 2006; Ouachani et al., 2013), only a 11–13 year periodicity was detected in precipitation. The five year cycles could be detected only in one of the precipitation time series included in the catchment average time series. This different periodic behaviour is likely caused by different geographical and climate conditions in the Danube Basin. Furthermore, catchment average precipitation time series were used instead of time series measured at a single climatic station in the above indicated studies. The global wavelet spectrum test of the climatic stations found long cycles in precipitation in the north eastern and south western segments of the analysed geographical area. These segments approximately correspond to the climatological regionalization according to Auer et al. (2007).

Similarly to Markovic and Koch (2013), no significant long cycles were found in the mean monthly temperature time series. This, however, differs from the findings of Andreo et al. (2006), who were able to detect long cycles in temperature. This may be attributed to the different climatic conditions – unlike in the upper Danube region, the temperatures on the Iberian peninsula analysed by Andreo et al. (2006) are strongly influenced by the Atlantic ocean and Mediterranean sea.

Long range dependence was found in all discharge time series. The presence of long range dependence in the Danube River discharges is in accordance with findings of Szolgayova et al. (2014) and Mudelsee (2007). Despite the fact that no long cycles could be detected in the temperature time series, all of these display long term persistence. Thus the long range dependence is likely driven by some other non-cyclical mechanism or process. No long range dependence could be found in monthly precipitation time series. This might indicate, that even though long cycles in precipitation do influence the Hurst coefficient of discharge, there are other significant factors, such as catchment storage characteristics, as suggested by Szolgayova et al. (2014).

The wavelet spectra of each of the observed time series were analysed as well. The high correlation between the respective time series contributes to the high degree of similarity between the spectra for each variable. In addition, the similarity between the temperature spectra is caused by the method of calculation of these time series. A visual decrease in the significant low frequency parts of the spectrum in the precipitation time series can be observed as we move downstream. This was accompanied by the decrease of the respective Hurst coefficients. Significant low frequency spots in the temperature spectra were observed for the years with daily temperature minima over years below the long time temperature average.

The relationships between precipitation, temperature and discharge time series were analysed using the cross-wavelet spectra and wavelet coherence. The precipitation–discharge wavelet coherence spectrum showed significant coherence for most of the periods at almost all time as would be expected. This is in agreement with the high consistency of precipitation and discharge decadal variability in the Danube basin found by Rimbu et al. (2002). The non-significant part of the wavelet coherence spectrum between precipitation and discharge ending in the early in the 1960s corresponds to the period, where almost no significant floods occurred on the Danube River (Blöschl and Montanari, 2010). This may be due to a regime switch in the precipitation time series.

A finding that is considered particularly interesting is the lead time between precipitation and discharge found from the cross wavelet spectra. At the period of four years, precipitation leads discharge by about six months. Soil moisture storage and near-surface groundwater have typical residence times of this order of magnitude. Interestingly, for the longer period of 11–14 years, the lead time is also longer (around 3 years). This suggests that deeper groundwater storage is accessed when long-term decadal fluctuations in precipitation and discharge occur which is not the case of the shorter term fluctuations. This can be clearly seen in Fig. 7 where a constant time lag has been used for generating discharge for all periods and consequently the lead time does not increase with the period. The effect of deeper groundwater storage is accessed is likely related to the non-linearity of the rainfall–runoff transformation which has been documented in numerous catchments around the world (e.g. Wittenberg, 1999). Furthermore, in the 1960s, the phase difference in the period of four years tends to decrease from six to one to two months. It is possible that this is also related to storage effects where shallower aquifers are accessed due to changes in the water balance.

A discharge convolution function was constructed in order to gain better understanding of the information provided by the wavelet spectra and the long range dependence in precipitation. The periodic behaviour of the discharge time series was acceptably reproduced using the convolution. The convolution results indicate that the long range dependence in discharge is partly influenced by the long range dependence in precipitation and partly by the non-linear catchment storage processes. It can be seen that the lead time of precipitation increases with the increasing weight of the long time kernel representing the rainfall–runoff relationship. This kind of convolution function could be used as a basis for a more sophisticated rainfall runoff wavelet based model, attempting to include and reproduce the phase shifts between the time series found in the cross-wavelet spectra (Kwon et al., 2007; Renaud et al., 2003).

The results show that especially mean monthly precipitation could be used in multivariate stochastic discharge time series modelling when considering a monthly time step, for example by means of a wavelet based model using wavelet decomposition and wavelet coherence in order to obtain a multivariate stochastic discharge model. Furthermore, additional wavelet analysis can be conducted in combination with other climate phenomena, such as the North Atlantic Oscillation in order to attribute the cycles found especially in precipitation and thus explain the found cyclical behaviour of the precipitation and temperature time series on larger scale. The findings of this paper give insights into the cyclical behaviour and changes of such behaviour of monthly discharge of the Danube River in central Europe and how these changes are influenced by precipitation and temperature in the respective catchment areas.

Acknowledgements

We would like to acknowledge financial support from the Austrian Science Funds (FWF) as part of the Vienna Doctoral Programme on Water Resource Systems (DK-plus W1219-N22). Analyses are based on stream flow data provided by the Global Runoff Data Centre. Furthermore we would like to acknowledge the data providers in the ECA&D project. Finally we would like to thank Rui Perdigao for his valuable inputs and insights and the reviewers for their helpful comments.

Appendix A. Hurst coefficient estimation

A.1. Regression on the periodogram

The regression on the periodogram is a method developed by Geweke and Porter-Hudak (1983) based on the idea that the periodogram of a time series follows the equation

$$\ln(I(\omega)) \sim c - d\ln(4\sin^2(\omega/2)) \quad (10)$$

where c is a constant and $I(\lambda)$ is the periodogram

$$I(\omega) = \frac{1}{2\pi N}\left|\left(\sum_{j=0}^{N-1} X_j e^{-ij\omega}\right)\right|^2 \quad \left\{\omega = \frac{2\pi k}{N}; \forall k = 1,\ldots,T\right\} \quad (11)$$

with $T = u_l\lfloor\frac{n-1}{2}\rfloor$ and the frequencies ω. Fitting a regression line on the logarithm of the frequencies and logarithm of the periodogram thus yields an estimate for d with $d = 1 - 2H$. In our case $u_l = 0, 1$ was used.

A.2. Detrended fluctuation analysis

The detrended fluctuation analysis (DFA) was introduced by Peng et al. (1994). In this paper the DFA of first order was used. Here the series of partial sums $Y_t = \sum_{i=1}^{t}(X_t - \overline{X})$ is divided into non-overlapping boxes of length l (where $\overline{X}$ is the mean of X_t). Then for each box a fluctuation function is calculated as

$$F(l) = \frac{1}{l}\sqrt{\sum_{i=1}^{l}(Y_i - ia - b)^2} \quad (12)$$

where $a, b \in \mathbb{R}$ are regression coefficients. This procedure is repeated for different values of l and a log–log plot of $F(l)$ against l is constructed. A generalized version of the Hurst coefficient is then obtained as the slope of the regression line. Here $H > 1$ indicates a non-stationary unbounded process (Peng et al., 1995).

References

Andreo, B., Jiménez, P., Durán, J.J., Carrasco, F., Vadillo, I., Mangin, A., 2006. Climatic and hydrological variations during the last 117–166 years in the south of the Iberian Peninsula, from spectral and correlation analyses and continuous wavelet analyses. J. Hydrol. 324, 24–39. http://dx.doi.org/10.1016/j.jhydrol.2005.09.010.

Auer, I., Böhm, R., Jurkovic, A., Lipa, W., Orlik, A., Potzmann, R., Schöner, W., Ungersböck, M., Matulla, C., Briffa, K., Jones, P., Efthymiadis, D., Brunetti, M., Nanni, T., Maugeri, M., Mercalli, L., Mestre, O., Moisselin, J.M., Begert, M., Müller-Westermeier, G., Kveton, V., Bochnicek, O., Stastny, P., Lapin, M., Szalai, S., Szentimrey, T., Cegnar, T., Dolinar, M., Gajic-Capka, M., Zaninovic, K., Majstorovic, Z., Nieplova, E., 2007. HISTALP – historical instrumental climatological surface time series of the Greater Alpine Region. Int. J. Climatol. 27, 17–46. http://dx.doi.org/10.1002/joc.1377.

Bataglia, F., Protopapas, M., 2011. Time-varying multi-regime models fitting by genetic algorithms. J. Time Ser. Anal. 32, 237–252. http://dx.doi.org/10.1111/j.1467-9892.2010.00695.x.

Blöschl, G., Montanari, A., 2010. Climate change impacts – throwing the dice? Hydrol. Process. 24, 374–381. http://dx.doi.org/10.1002/hyp.7574.

Dingman, S.L., 2008. Physical Hydrology. Waveland Press, Inc., Long Grove.

Elek, P., Markus, L., 2007. A light-tailed conditionally heteroscedastic model with applications to river flows. J. Time Ser. Anal. 29, 14–36. http://dx.doi.org/10.1111/j.1467-9892.2007.00542.x.

Fisher, A., Green, D., Metcalfe, A., 2012. Modelling of hydrological persistence for hidden state markov decision processes. Ann. Oper. Res. 199, 215–224. http://dx.doi.org/10.1007/s10479-011-0992-2.

Frolov, A.V., 2011. Discrete dynamic–stochastic model of long term river runoff variations. Water Resour. 38 (5), 583–592. http://dx.doi.org/10.1134/S0097807811040051.

Gelati, E., Madsen, H., Rosjberg, D., 2010. Markov-switching model for nonstationary runoff conditioned on El Nino information. Water Resour. Res. 46, W02517. http://dx.doi.org/10.1029/2009WR007736.

Geweke, J., Porter-Hudak, S., 1983. The estimation and application of long memory time series models. J. Time Ser. Anal. 4 (4), 221–238, doi:0.1111/j.1467-9892.1983.tb00371.x.

Grau-Carles, P., 2005. Tests of long memory: a bootstrap approach. Comput. Econ. 25, 103–113. http://dx.doi.org/10.1007/s10614-005-6277-6.

GRDC. Global Runoff Data Center – Dataset of River Discharge Time Series. Koblenz, Germany, 2011.

Grinsted, A., Moore, J.C., Jevrejeva, S., 2004. Application of the cross wavelet transform and wavelet coherence to geophysical time series. Nonlinear Process. Geophys. 11, 561–566. http://dx.doi.org/10.5194/npg-11-561-2004.

Hurell, J.W., 1995. Decadal trends in the North Atlantic Oscillation: regional temperatures and precipitation. Science 269, 676–679. http://dx.doi.org/10.1126/science.269.5224.676.

Kaiser, G., 1994. A Friendly Guide to Wavelets. Birkhäuser, Berlin.

Klein Tank, A.M.G., Wijngaard, J.B., Können, G.P., Böhm, R., Demaré, G., Gocheva, A., Mileta, M., Pashiardis, S., Hejkrlik, L., Kern Hansen, C., Heino, R., Bessemoulin, P., Müller Westermeier, G., Tzanakou, M., Szalai, S., Pálsdóttir, T., Fithzgerald, D., Rubin, S., Capaldo, M., Maugeri, M., Leitass, A., Bukantis, A., Aberfeld, R., van Engelen, A.F.V., Forland, E., Mietus, M., Coehlo, F., Mares, C., Razuzaev, V., Nieplova, E., Cegnar, T., Antonio López, J., Dahlström, B., Moberg, A., Kirchhofer, W., Ceylan, A., Pachuliuk, O., Alexander, L.V., Petrovic, P., 2003. Daily dataset of 20th-century surface air temperature and precipitation series for the European Climate Assessment. Int. J. Climatol. 22, 1441–1453. http://dx.doi.org/10.1002/joc.773, <http://www.ecad.eu>.

Komorníková, M., Szolgay, J., Svetlíková, D., Szökeová, D., Jurčák, S., 2008. A hybrid modelling framework for forecasting monthly reservoir inflows. J. Hydrol. Hydromech. 56 (3), 145–162. http://dx.doi.org/10.1111/j.1467-9892.2010.00695.x.

Kwon, H.-H., Lall, U., Khalil, A.F., 2007. Stochastic simulation model for nonstationary time series using an autoregressive wavelet decomposition:

applications to rainfall and temperature. Water Resour. Res. 43 (5), W05407. http://dx.doi.org/10.1029/2006WR005258.
Labat, D., 2008. Wavelet analysis of the annual discharge records of the world's largest rivers. Adv. Water Resour. 31, 109–117. http://dx.doi.org/10.1016/j.advwatres.2007.07.004.
Lafreniere, M., Sharp, M., 2003. Wavelet analysis of inter-annual variability in the runoff regimes of glacial and nival stream catchments, Bow Lake, Alberta. Hydrol. Process. 17, 1093–1118. http://dx.doi.org/10.1002/hyp.1187.
Lee, T., 2012. Serial dependence properties in multivariate streamflow simulation with independent decomposition analysis. Hydrol. Process. 26, 961–972. http://dx.doi.org/10.1002/hyp.8177.
Liu, H.-L., Bao, A.-M., Chen, X., Wang, L., Pan, X.-I., 2011. Response analysis of rainfall–runoff processes using wavelet transform: a case study of the alpine meadow belt. Hydrol. Process. 25, 2179–2187. http://dx.doi.org/10.1002/hyp.7969.
Mallat, S., 1998. A Wavelet Tour of Signal Processing. Academic Press, New York.
Mann, M.E., Lall, U., Salzman, B., 1995. Decadal-to-centennial-scale climate variability: insights into the rise and fall of the Great Salt Lake. Nonlinear Process. Geophys. 22 (8), 937–940. http://dx.doi.org/10.1029/95GL00704.
Maraun, D., Kurths, J., 2004. Cross wavelet analysis: significance testing and pitfalls. Nonlinear Process. Geophys. 11, 505–514. http://dx.doi.org/10.5194/npg-11-495-2004.
Markovic, D., Koch, M., 2013. Long-term variations and temporal scaling of hydroclimatic time series with focus on the german part of the Elbe River Basin. Hydrol. Process. 2200, 14410–14530. http://dx.doi.org/10.1002/hyp.9783.
Massei, N., Laignel, B., Deloffre, J., Mesquita, J., Motelay, A., Lafite, R., Durand, A., 2010. Long-term hydrological changes of the Seine River flow (France) and their relation to the North Atlantic Oscillation over the period 1950–2008. Int. J. Climatol. 30, 2146–2154. http://dx.doi.org/10.1002/joc.2022.
Modarres, R., Ouarda, T.B.M.J., 2013. Modeling rainfall–runoff relationship using multivariate GARCH model. J. Hydrol. 499, 1–18.
Montanari, A., Rosso, R., Taqqu, M.S., 2000. A seasonal fractional ARIMA model applied to the Nile River monthly flows at Aswan. Water Resour. Res. 36 (5), 1249–1259. http://dx.doi.org/10.1029/2000WR900012.
Mudelsee, M., 2007. Long memory of rivers from spatial aggregation. Water Resour. Res. 43, W01202. http://dx.doi.org/10.1029/2006WR005721.
Osborn, T.J., Briffa, K.R., Tett, S.F.B., Jones, P.D., Trigo, R.M., 1999. Evaluation of the North Atlantic Oscillation as simulated by a climate model. Climate Dyn. 15, 685–702. http://dx.doi.org/10.1007/s003820050310.
Ouachani, R., Bargaoui, Z., Ouarda, T., 2013. Power of teleconnection patterns on precipitation and streamflow variability of upper Medjerda Basin. Int. J. Climatol. 33 (1), 58–76. http://dx.doi.org/10.1002/joc.3407.
Pekárová, P., Miklánek, P., Pekár, J., 2003. Spatial and temporal runoff oscillation analysis of the main rivers of the world during the 19th–20th centuries. J. Hydrol. 274, 62–79. http://dx.doi.org/10.1016/S0022-1694(02)00397-9.
Peng, C.K., Buldyrev, S.V., Havlin, S., Simons, M., Stanley, H.E., Goldberger, A.L., 1994. Mosaic organization of dna nucleotides. Phys. Rev. E 49, 1685–1689. http://dx.doi.org/10.1103/PhysRevE.49.1685.
Peng, C.K., Havlin, S., Stanley, H.E., Goldberger, A.L., 1995. Quantification of scaling exponents and crossover phenomena in nonstationary heartbeat time series. Chaos 5 (1), 82–87. http://dx.doi.org/10.1063/1.166141.
Pires, C.A., Perdigao, R.A.P., 2007. Non-Gaussianity and asymmetry of the winter monthly precipitation estimation from the NAO. Mon. Wea. Rev. 135, 430–448. http://dx.doi.org/10.1175/MWR3407.1.
Probst, J.L., Tardy, Y., 1987. Long range streamflow and world continental runoff fluctuations since the beginning of this century. J. Hydrol. 94, 289–311. http://dx.doi.org/10.1016/0022-1694(87)90057-6.
Renaud, O., Starck, J., Murtagh, F., 2003. Prediction based on multiscale decomposition. Int. J. Wavelets Multi 1, 217–232.
Rimbu, N., Boronenat, C., Bruta, C., Dima, M., 2002. Decadal variability of the Danube River flow in the lower basin and its relation with the north atlantic oscillation. Int. J. Climatol. 22, 1169–1179. http://dx.doi.org/10.1002/joc.788.
Rogers, J.C., 1997. North Atlantic storm track variability and its association to the North Atlantic Oscillation and climate variability of northern Europe. J. Climate 10, 1635–1647.
Sang, Y.F., 2013. A review on the applications of wavelet transform in hydrology time series analysis. Atmos. Res. 122, 8–15. http://dx.doi.org/10.1016/j.atmosres.2012.11.003.
Skoien, J.O., Blöschl, G., Western, A.W., 2003. Characteristic space scales and timescales in hydrology. Water Resour. Res. 39 (10), W01304. http://dx.doi.org/10.1029/2002WR001736.
Szolgayova, E., Laaha, G., Blöschl, G., Bucher, C., 2014. Factors influencing long range dependence in streamflow of European rivers. Hydrol. Process. 28, 1573–1586. http://dx.doi.org/10.1002/hyp.9694.
Timuhins, A., Rodinovs, V., Klavins, M., 2010. Wavelet analysis of the baltic region river runoff long-term trends and fluctuations. Proc. Latvian Acad. Sci. 64 (5/6), 229–235. http://dx.doi.org/10.2478/v10046-011-0009-1.
Torrence, C., Compo, G., 1999. A practical guide to wavelet analysis. Bull. Am. Meteorol. Soc. 79, 61–78.
Torrence, C., Webster, P.J., 1999. Interdecadal changes in the ENSO-monsoon system. J. Climate 12, 2679–2690.
Valent, P., Howden, N., Szolgay, J., Komorníková, M., 2011. Analysis of nitrate concentrations using nonlinear time series models. J. Hydrol. Hydromech. 59 (3), 157–170. http://dx.doi.org/10.2478/v10098-011-0013-9.
Vidakovic, B., 1999. Statistical Modelling by Wavelets. John Wiley & Sons, New York.
Wittenberg, H., 1999. Baseflow recession and recharge as nonlinear storage processes. Hydrol. Process. 13, 715–726. http://dx.doi.org/10.1002/(SICI)1099-1085(19990415)13:5<715::AID-HYP775>3.0.CO;2-N.
Yusof, F., Kane, I.L., Yusop, Z., 2013. Structural break or long memory: an empirical survey on daily rainfall data sets across Malaysia. Hydrol. Earth Sys. Sci. 17, 1311–1318. http://dx.doi.org/10.5194/hess-17-1311-2013.